The Impact of Greenhouse Climate Change on the Energetics and Hydrologic Processes of Mid-latitude Transient Eddies

Lee E. Branscome

Environmental Dynamics Research, Inc.

7338 155th Place North

Palm Beach Gardens, FL 33418, USA

William J. Gutowski, Jr.

Atmospheric and Environmental Research, Inc.

840 Memorial Drive

Cambridge, MA 02139, USA

May 1991

Send proofs to Lee E. Branscome

Telephone: 407 744-4889

Fax: 407 744-5098

Abstract

Atmospheric transient eddies contribute significantly to mid-latitude energy and water vapor transports. Changes in the global climate, as induced by greenhouse enhancement, will likely alter transient eddy behavior. Unraveling all the feedbacks that occur in general circulation models (GCM's) can be difficult. Here we isolate the transient eddies from the feedbacks and focus on the response of the eddies to zonal-mean climate changes that result from CO_2-doubling. Using a primitive-equation spectral model, we examine the impact of climate change on the life cycles of transient eddies. We compare transient eddy behavior in experiments with initial conditions that are given by the zonal-mean climates of GCM's with current and doubled amounts of CO_2.

The smaller meridional temperature gradient in a doubled CO_2 climate leads to a reduction in eddy kinetic energy, especially in the subtropics. The decrease in subtropical eddy energy is related to a substantial reduction in equatorward flux of eddy activity during the latter part of the life cycle. The reduction in equatorward energy flux alters the moisture cycle. Eddy meridional transport of water vapor is shifted slightly poleward and subtropical precipitation is reduced. The water vapor transport exhibits a relatively small change in magnitude, compared to changes in eddy energy, due to the compensating effect of higher specific humidity in the doubled-CO_2 climate. An increase in high-latitude precipitation is related to the poleward shift in eddy water vapor flux. Surface evaporation amplifies climatic changes in water vapor transport and precipitation in our experiments.

1 Introduction

Experiments with general circulation models (GCM's) indicate that increases in atmospheric carbon dioxide and other greenhouse gases will cause an increase in global surface temperature. Changes in the hydrologic cycle are also anticipated. For example, GCM experiments generally show that an increase in CO_2 will lead to increased precipitation, especially in the extratropics (Schlesinger and Mitchell 1987). Total water vapor content of the atmosphere also increases in the GCM experiments. The amount and distribution of water in the atmosphere plays a critical role in global climate, primarily through its effect on radiative processes. The anticipated increase in water vapor content will contribute significantly to the global warming process by enhancing the greenhouse effect (Hansen et al. 1984). In addition, changes in the hydrologic cycle will influence distributions of cloud, ice, and snow cover which affect the global radiative budget.

Because water in its various forms is a key element of the climate system, it is important to understand the processes that contribute to the hydrologic cycle and how they might be affected by global warming. Atmospheric transient eddies are an integral part of the global water balance. In the Northern Hemisphere transient eddies are responsible for about two-thirds of the poleward water vapor transport in mid-latitudes (Oort 1983). Their contribution to total transport is even greater in the Southern Hemisphere. Furthermore, most of the wintertime extratropical precipitation is associated with transient eddies. Water vapor

transport by transient eddies is also an important component of the global energy budget. Latent heat transport by transient eddies contributes about 30% of the total heat transport in mid-latitudes in Northern Hemisphere winter and about 50% in summer as derived from Oort's (1983) data. In the Southern Hemisphere the contribution of latent heat flux by transient eddies is even more significant (Michaud and Derome 1991).

The transient eddies responsible for these transports have horizontal scales of 1000-10,000 km and are generated primarily by the baroclinic instability of the large-scale zonal flow. Changes in the large-scale flow, as induced by an increase in CO_2 and other greenhouse gases, will likely alter the behavior of transient eddies and their sensible and latent heat transports. GCM's contain a myriad of feedbacks that determine the total response of these models to CO_2-doubling. Unraveling the effects of all the feedbacks can be difficult. Our purpose here is to isolate the behavior of atmospheric transient eddies from the feedbacks and focus on the response of the eddies to overall changes in climate that result from CO_2-doubling. We use this approach to assess the contribution of transient eddies to the climate change. Thus, our work can be viewed as an open-loop study of the response of transient eddies to CO_2-induced climate change.

We accomplish our purpose by studying eddy life cycle simulations in a primitive-equation spectral model. Life cycle simulations, using the current climate's zonal average state for initial conditions, are highly informative about the behavior of atmospheric eddies (Gall 1976; Simmons and Hoskins 1978;

Branscome et al. 1989; Gutowski et al. 1989; Gutowski et al. 1991a). We examine the impact of climate change on eddy life cycles by using the zonal-mean climates of GCM's with current and doubled amounts of CO_2 as initial conditions for our experiments. We compare the eddy kinetic energy, water vapor flux, and precipitation that are generated during the eddy life cycles in the two different climates. We also evaluate the influence of surface evaporation on eddy transport in the two climates. Due to the short-term nature of our experiments, changes in eddy evolution are caused by changes in the zonal-mean climate only and are isolated from other feedbacks present in complete GCM simulations.

In the next section we describe the model and experimental design in more detail. In the third section we give an overview of the effect of climate change on wave evolution, eddy transports of sensible heat and water vapor, and precipitation. We also discuss the effect of model resolution on wave behavior. In the fourth section we distinguish the individual effects of CO_2-induced changes in temperature, humidity and surface evaporation on the eddy's water vapor transport and precipitation. In the fifth section we compare our results with a parameterization of water vapor flux proposed by Stone and Yao (1990). Some conclusions are presented in the final section.

2 Model and experiments

Here we give a brief description of the model; a more detailed description is contained in Branscome et al. (1989) and Gutowski et al. (1991a). The model is

a primitive equation, global spectral model (GSM) adapted from the National Meteorological Center's (NMC's) GSM (Sela 1980; Brenner et al. 1982). The model uses Bourke's (1974) representation of the spectral prognostic equations, which is the same approach used in the National Center for Atmospheric Research Community Climate Model (NCAR CCM) described by Pitcher et al. (1983) and used by NCAR for doubled-CO_2 experiments (Washington and Meehl 1984). The model has 10 sigma layers of equal thickness to resolve vertical structure. Test computations using 20 layers gave negligibly different results.

Because our study is limited to the effect of changes in the zonal mean state on transient eddy evolution, we use a simple configuration of the model. The surface is zonally uniform and flat, so that no time-mean stationary eddies are generated. Surface sensible heat flux, moisture flux, and momentum drag are computed using bulk formulae with a surface drag coefficient of $C_D = 0.002$. The temperature of the lower boundary is fixed throughout the integration at the initial temperature of the lowest atmospheric layer. The lower boundary is moist and, therefore, acts like a sea surface. Significant sensible and latent heat fluxes occur only after the eddy becomes strong enough to change the lowest-layer temperature and moisture distributions.

Like GCM's the model contains two condensation mechanisms: large-scale, stable precipitation and moist convection. The stable precipitation is the same as that used in the original NMC GSM (Phillips 1979; Brenner et al. 1982). This type of condensation occurs when a model layer becomes supersaturated, usually

by large-scale uplift. Our parameterization for convection is an implementation of Kuo's (1974) scheme, using a closure assumption for Kuo's *b* parameter given by Krishnamurti et al. (1976).

We perform all experiments with zonal wavenumber 7 and its two higher harmonics, 14 and 21. Results from test computations indicate that retaining these two harmonics is more than sufficient for resolving the life cycle of an eddy whose fundamental scale is wavenumber 7 (Gutowski et al. 1991a). We expect that wavenumber 7 and waves of similar synoptic scale are responsible for most of the transient eddy flux of water vapor in the extratropics. Similar life cycle simulations with wavenumber 4 generate eddy water vapor flux that is only one-third as large as the flux in wavenumber 7 experiments (Gutowski et al. 1991a). Furthermore, synoptic-scale waves dominate sensible heat flux and baroclinic energy conversions by transient eddies (Blackmon and White 1982; Ulbrich and Speth 1991). Thus, we consider wavenumber 7 and its higher harmonics to be representative wavenumbers for the processes under investigation.

We initialize our model by adding a wave perturbation in the temperature field to the zonal mean state. The temperature perturbation has an amplitude of 0.1° C in the lowest layer and an exponential decrease with height intended to simulate the structure of an unstable Charney mode. For each zonal wavenumber, the model uses 15 meridional modes to resolve latitudinal structure. Because we run the model with hemispheric symmetry, this amounts to a global truncation equivalent to rhomboidal 30 for each zonal wavenumber. Note that the smallest

scales in our experiments are somewhat shorter than those resolved in many GCM climate experiments.

We perform several short-term integrations with initial conditions given by zonally averaged, time-mean states generated by GCM climate simulations. Wintertime climatic conditions for present-day and doubled CO_2 amounts are taken from experiments with the Geophysical Fluid Dynamics Laboratory (GFDL) GCM (Manabe and Wetherald 1987) and NCAR CCM (Washington and Meehl 1984). By limiting our experiments to the short-term evolution of mid-latitude eddies, the eddy contribution to the hydrologic cycle is isolated from other feedbacks, allowing us to concentrate on how dynamical transports by transient eddies respond to climate change. By changing the initial conditions, model resolution, or boundary conditions in our experiments, we can assess the impact of certain processes and modeling procedures on eddy evolution and water vapor transport.

The upper half of Fig. 1 shows the zonally averaged, time-mean 950 hPa temperature during Northern Hemisphere winter in the GFDL and NCAR GCM's for the present-day CO_2 amount ($1xCO_2$). The difference in temperature between the $1xCO_2$ and doubled-CO_2 ($2xCO_2$) simulations is shown in the lower half of Fig. 1. The increase near the pole is larger in the GFDL GCM than in the NCAR model because changes in sea ice coverage are larger in the GFDL model (Gutowski et al. 1991b). Note that the largest temperature increase due to CO_2-doubling occurs in high latitudes, thus reducing the equator-to-pole temperature

difference. Because the meridional temperature gradient in mid-latitudes is smaller in the $2xCO_2$ experiments, less potential energy is available in the zonal mean state for conversion to eddy kinetic energy through baroclinic instability.

Fig. 2 (upper half) shows the vertically and zonally averaged specific humidity for northern winter from the GFDL and NCAR $1xCO_2$ simulations. The lower half of Fig. 2 shows the change in specific humidity due to CO_2-doubling. Relative humidity is largely unchanged in the two GCM's when the amount of CO_2 is doubled. Thus, an increase in specific humidity, Q, is coincident with the global temperature increase. The effect is largest in the tropics where the mean temperature is highest.

The temperature and humidity profiles in Figs. 1 and 2 constitute part of the background mean states that are used to initialize our experiments. The vertical structures of the temperature and humidity fields are also obtained from the GFDL and NCAR GCM experiments. We obtain the initial states for the zonal wind which balances the temperature fields by the method described in Branscome et al. (1989). The balance calculation for the zonal wind ensures that no meridional motion develops in the absence of wave activity and the initial state is a steady, zonally symmetric solution of the model's equations.

3 Effect of climate change on eddy energetics and transports

Starting from the small initial perturbation in the temperature field of the

fundamental wavenumber, a disturbance grows at the expense of the available potential energy in the initial zonal mean state and begins to modify the zonal circulation. Once the wave disturbance or eddy depletes its baroclinic energy source and dissipation acts on the wave, the eddy reaches a maximum amplitude. Frictional dissipation and barotropic conversion of eddy kinetic energy (EKE) to zonal mean kinetic energy eventually lead to a decrease in EKE. Thus, an eddy "life cycle" can be defined. The eddy evolution is similar to the life cycles in a dry atmosphere as investigated by Simmons and Hoskins (1978) and Branscome et al. (1989). Gutowski et al. (1991a) give a complete view of eddy life cycles and transports in a moist atmosphere.

The evolution of EKE in our experiments is shown in Fig. 3. Note that the maximum EKE is smaller in the experiments that use initial states taken from the $2xCO_2$ GCM simulations. Similarly, the poleward flux of sensible heat by the eddy (not shown) is about 25% smaller in our experiments with the $2xCO_2$ climates. These results are consistent with the findings of Manabe and Wetherald (1975, 1980) in their GFDL GCM climate experiments. Amplitudes attained by transient eddies depend on the amount of available potential energy in the zonal mean state (Schneider 1981). Less potential energy is available to the growing disturbance in the $2xCO_2$ experiments, so the maximum energy reached by the disturbance is smaller than in the $1xCO_2$ experiments.

During the early stage of eddy growth (the first 14 days of the integrations in Fig. 3), the eddies in the $1xCO_2$ and $2xCO_2$ experiments have a similar structure

with a maximum in EKE at 45° N. As indicated in Fig. 3, the eddy in the $1xCO_2$ experiment grows more rapidly because of the larger meridional temperature gradient in the $1xCO_2$ climate. As the eddies mature, eddy activity is transported from mid-latitudes into the subtropics by an Eliassen-Palm (EP) flux. An example of this behavior is also found in Edmon et al. (1980). The direction of the EP flux is indicative of the direction of wave energy propagation (Edmon et al. 1980).

The equatorward EP flux increases eddy activity in the subtropics, which is reflected in an amplification of subtropical eddy energy during the latter stage of eddy growth (days 16-20 of the integrations in Fig. 3). In the $2xCO_2$ experiments the eddy converts less potential energy from the zonal mean state in mid-latitudes and exports less eddy activity to the subtropics than the eddy in the $1xCO_2$ experiments. When the eddy reaches its maximum amplitude, the subtropical EKE in the $2xCO_2$ climate is substantially smaller than the subtropical EKE in the $1xCO_2$ case. The subsequent change in the latitudinal distribution of EKE is shown in Fig. 4 for the experiments using the NCAR CCM climates as initial conditions. Similar behavior was found in our experiments with the GFDL climates. Thus, the climatic change in the latitudinal distribution of EKE is not the result of a change in the unstable linear wave structure, but the result of a change in the nonlinear evolution of the eddy.

The meridional flux of specific humidity (water vapor) by the eddy is shown in Fig. 5. The flux is zonally and vertically averaged, and averaged again over the

lifetime of the disturbance. The observed transient eddy flux from Northern Hemisphere winter (Oort 1983) is also shown and generally agrees with the simulated flux. This agreement is consistent with our assumption that transient eddies with the horizontal scales similar to the wavenumbers used in our experiments are responsible for most of the poleward transport by extratropical eddies.

Even though eddy kinetic energy (Figs. 3 and 4) and eddy flux of sensible heat are considerably smaller in the $2xCO_2$ experiments, the magnitude of eddy water vapor flux does not decrease when CO_2 is doubled. As suggested by Manabe and Wetherald (1975), a reduction in eddy meridional velocity, evidenced by the decrease in EKE, is offset by the global increase in water vapor in the doubled CO_2 climate. Nevertheless, the latitudinal distribution of the flux is altered by the climate change. With an increase of flux in high latitudes and a decrease in the subtropics, the eddy flux of water vapor shifts poleward when CO_2 is doubled. The poleward shift is primarily related to the change in the latitudinal distribution of EKE and the general increase in water vapor in the $2xCO_2$ climate. Poleward of 50° N the eddy velocity variance is unchanged between the $1xCO_2$ and $2xCO_2$ climates (Fig. 4). Coupled with the global increase in specific humidity in the $2xCO_2$ climate, the water vapor flux increases in middle and high latitudes. At lower latitudes the flux decreases because the increase in specific humidity does not entirely compensate for the substantial reduction in eddy velocity variance in the subtropics. We examine these competing effects in more detail in the next section.

The eddy generates a mean meridional circulation (MMC) during its life cycle. The strength of the eddy-induced MMC depends largely on the poleward eddy flux of momentum in the subtropics. The water vapor transport by the MMC is poleward from 25° to 60°N and equatorward in the tropics. Thus, the direction of the MMC transport in our experiments is same as the Ferrel and Hadley cell transports in the atmosphere. The magnitude of the water vapor transport by the Ferrel cell decreases when CO_2 is doubled in our experiments, reflecting the substantial reduction in subtropical eddy momentum flux. The reduction in the strength of the Ferrel cell circulation outweighs the increase in specific humidity in determining the change in the water vapor transport by the cell. Fig. 5 shows only the eddy flux of water vapor. If we include the MMC transport (Fig.6), we find that the changes in total water vapor transport are not as large as the changes seen in the eddy flux (Fig. 5). Thus, the mid-latitude MMC water vapor transport induced by the eddy provides a modest negative feedback to the eddy transport.

The amount of precipitation due to large-scale, non-convective condensation during the eddy lifetime is shown in Fig. 7. Consistent with the poleward shift in eddy moisture flux and reduction in subtropical eddy energy, large-scale precipitation shifts poleward when CO_2 is doubled. The reduction in large-scale precipitation equatorward of 40° N is due to a decrease in eddy vertical motion and subsequent reduction in mid-tropospheric condensation. Furthermore, condensation in the lower troposphere, which is related to surface heat and moisture exchange, is also reduced. The change in low-level precipitation is

examined in more detail in the next section. In high latitudes the increase in precipitation is related to the increase in large-scale moisture flux convergence (Fig. 5).

Convective precipitation induced by the eddies in our experiments is smaller than the large-scale precipitation and limited to the subtropics and tropics. Fig. 8 shows the convective precipitation induced by the eddy in our experiments using the NCAR climate states. A significant reduction occurs when the CO_2 is doubled, reflecting the decrease in eddy kinetic energy and low-level moisture convergence in the subtropics and tropics. In our experiments with GFDL climates the convective precipitation is generally smaller than in the NCAR cases and the reduction due to CO_2 doubling is not quite as large as the decrease seen in Fig. 8. Because tropical rainfall is not generally associated with the development of baroclinic waves in mid-latitudes, our experiments do not adequately model all tropical precipitation. However, the experiments suggest a reduction in convective precipitation associated with mid-latitude eddies.

The partitioning of precipitation into convective and large-scale components in our life cycle experiments may not be the same as in the complete GCM climate simulations. Furthermore, the partitioning of precipitation in GCM's may be very sensitive to the choice of convective parameterization, although the total precipitation may not change significantly (Stone and Yao 1991). We performed a few experiments with a different convective scheme (a modified Arakawa-Schubert parameterization described by Grell et al. 1991) and found no substantial

differences from our standard experiments with the Kuo scheme. Considering the uncertainty about the partitioning of precipitation, the climate change in total precipitation is perhaps more important to examine in our experiments. If we consider the total precipitation as represented by the sum of Figs. 7 and 8, we note a clear reduction in the subtropics and an increase in high latitudes. The change in total precipitation in our experiments generally agrees with the redistribution of zonal-mean wintertime precipitation found in GCM simulations of CO_2-induced climate change (Schlesinger and Mitchell 1987; Manabe and Wetherald 1985).

We also examined the impact of model resolution on the latitudinal changes in water vapor transport and precipitation. Specifically, we reduced the resolution in two experiments by retaining half as many meridional modes so that the meridional resolution is similar to the resolution used in many GCM climate simulations. Water vapor transport and precipitation from two experiments using the GFDL climates are shown in Fig. 9. Note that the water vapor flux shows a noticeable increase when CO_2 is doubled, unlike the results of the more highly resolved experiments (Fig. 5). Changes in precipitation are small and do not resolve the poleward shift seen in Fig. 7. The results show that the simulation of the eddy-induced hydrologic cycle and its response to CO_2 doubling may be quite sensitive to model resolution.

4 Impact of changes in temperature, humidity and surface evaporation on eddy behavior

In a few special experiments we compare the importance of the increase of specific humidity and the decrease of meridional temperature gradient on water vapor transport and precipitation. The initial conditions are taken from the GFDL GCM only. In one of these experiments ("ΔT Only") the initial state consists of the temperature from the $2xCO_2$ climate and the specific humidity of the $1xCO_2$ climate. Warm surface temperatures in the $2xCO_2$ climate, coupled with low specific humidity in the lowest layer of the $1xCO_2$ climate, would cause a large flux of water vapor into the model's lowest layer during the first day of integration in the "ΔT Only" case. Therefore, we prevent surface evaporation in the "ΔT Only" experiment. For purposes of comparison, surface evaporation is also excluded from two experiments, $1xCO_2$-NE and $2xCO_2$-NE, that use the complete $1xCO_2$ and $2xCO_2$ climates as initial conditions, respectively. Thus, water vapor transport and precipitation are influenced only by changes in the initial states of atmospheric temperature and humidity .

Fig. 10 shows water vapor flux and large-scale precipitation in the three experiments described above. Comparing the water vapor flux in the "ΔT Only" case with the $1xCO_2$-NE experiment (the initial conditions in "ΔT Only" and $1xCO_2$-NE differ in temperature only), we see that the water vapor flux is smaller in the subtropics and unchanged in high latitudes in the "ΔT Only" case. These results are consistent with our earlier conclusion that the climate change in

meridional temperature gradient leads to a reduction in the subtropical EKE which, in turn, causes a decrease in eddy water vapor transport. When the CO_2-induced increase in specific humidity is included in the initial state (the $2xCO_2$-NE case), the water vapor transport increases in magnitude compared to the "ΔT Only" case. Thus, the increase in mean-state specific humidity compensates for the reduction in flux caused by the decrease in meridional temperature gradient. As discussed earlier, the net effect of climate changes in temperature and humidity is a slight poleward shift in the eddy flux of water vapor.

Compared to the $1xCO_2$-NE case, precipitation in the "ΔT Only" case is much smaller and shifted poleward. Associated with the reduced eddy energy in the "ΔT Only" case is a reduction in eddy vertical motion, causing less large-scale uplift and, hence, less precipitation. In addition, the initial relative humidity in the "ΔT Only" case is smaller than in the $1xCO_2$-NE experiment, simply because the initial specific humidity is the same in the two cases, but the global temperature is higher in the "ΔT Only" experiment. Therefore, the supersaturation required for large-scale precipitation is not as readily achieved by the eddy in the "ΔT Only" experiment as in the $1xCO_2$-NE case. By including the CO_2-induced change in specific humidity, precipitation in the $2xCO_2$-NE case increases substantially compared to the "ΔT Only" case. An increase in specific humidity can enhance condensational heating which may cause stronger vertical motions and more precipitation in baroclinic eddies (Gutowski et al. 1991a). However, we found that eddy vertical motions are not significantly different in the "ΔT Only" and $2xCO_2$-NE experiments. Therefore, the increase in precipitation from the "ΔT

Only" case to the $2xCO_2$-NE experiment is primarily due to the enhancement of water vapor content, rather than an amplification of vertical motions by latent heat release.

When surface evaporation is excluded from our experiments, precipitation amounts are cut in half (cf. top of Fig. 7 and bottom of Fig. 10, noting the different scales for precipitation). As a result, precipitation changes between the $1xCO_2$-NE and $2xCO_2$-NE experiments in Fig. 10 are smaller than the changes in experiments with surface evaporation (Fig. 7). Thus, part of the change in precipitation induced by CO_2 doubling is linked to the interaction of the eddy and surface evaporation. Most of the eddy-induced surface evaporation occurs in the subtropics. When low-level moist air from the subtropics is advected poleward by the eddy, it becomes supersaturated as it passes over the cold lower boundary of mid-latitudes. Because eddy energy in the subtropics is significantly reduced in the $2xCO_2$ climate, the combined process of eddy-induced surface evaporation, poleward advection of moist air, and low-level supersaturation is diminished.

5 Comparison with a parameterization of water vapor flux

Climate models which are simpler, but computationally more efficient than GCM's, usually do not include the global hydrologic cycle. Stone and Yao (1990) have proposed a parameterization of transient eddy water vapor transport, which can be used in one-dimensional (latitude only) and two-dimensional (latitude vs. height) climate models. Their parameterization is based on baroclinic

instability theory, combined with scaling arguments for wave amplitudes and assumptions about moisture distribution. In Stone and Yao's parameterization the meridional and vertical flux of water vapor flux depends on zonally averaged temperature and humidity fields. Derived from formulations by Leovy (1973) and Branscome (1983), it is perhaps the only theoretically-based parameterization of water vapor transport by large-scale eddies. Stone and Yao (1990) used the parameterization in a two-dimensional climate model and found good agreement between the parameterized flux and explicitly calculated transport in a three-dimensional version of their model.

One- and two-dimensional climate models can provide valuable initial assessments of climate sensitivity. For this reason, we compare the sensitivity of moisture transport in our experiments with Stone and Yao's parameterized flux, using the zonal mean climate of the GFDL GCM as input for their parameterization. Results using the NCAR climate as input for the parameterization are very similar. Fig. 11 shows the vertically averaged meridional flux as a function of latitude from the parameterization and our experiments. Fig. 12 shows the vertical profile of meridional flux at 30° N along with the observed eddy flux. The parameterization's response to CO_2-induced changes in the zonal mean state is small, reflecting the compensating effects of a reduced temperature gradient and an increased water vapor content. Similar compensation occurs in our numerical experiments.

The parameterization generally overestimates the meridional flux in the

subtropics and lower troposphere compared to the eddy flux from observations and our experiments. The structure of the GFDL and NCAR climates tends to exaggerate the latitudinal confinement of the parameterized flux. The GFDL and NCAR climates have meridional temperature gradients that are stronger in the subtropics and weaker in higher latitudes than the observed temperature gradient. The water vapor flux parameterization is based on a sensible heat flux parameterization (Branscome 1983) that is strongly dependent on meridional temperature gradient. Small changes in temperature gradient lead to relatively large changes in the parameterized flux. Thus, the parameterized flux, using the GFDL or NCAR climate as input, is confined to the region with a large temperature gradient, i.e., the subtropics.

Changes in wave structure due to nonlinear dynamics are also responsible for the disprecancy between the meridional extent of the water vapor flux in our model and the parameterization. If we examine our model's flux during the first half of the growth stage, we find that the flux is sharply peaked near 30° N in agreement with the latitudinal distribution of the parameterization in Fig. 11. Once the eddy reduces the moisture in the subtropics and increases it in high latitudes, we find that the moisture flux maximum in the model moves poleward and the flux is more evenly distributed across mid-latitudes. Thus, the considerable change in the latitudinal distribution of the flux that occurs as the eddy and zonal mean state evolve may not be adequately represented in the parameterization.

The discrepancy in the vertical structure of the flux (Fig. 12) is likely due to boundary layer processes. The parameterization has a simple representation of the boundary layer which diminishes the meridional flux near the lower boundary. The vertical scale of the boundary layer is chosen by Stone and Yao (1990) as 450m in the parameterization. If that scale is doubled, then the flux in the lower troposphere has a structure more like the flux in our integrations. In an experiment without surface friction, the meridional flux in our model is largest in the lowest layer and has the sharp exponential decay seen in the parameterized flux of Fig. 12. Because the water vapor flux is confined to the lower troposphere, any parameterization of the flux must account for boundary layer effects and may be sensitive to details of the boundary layer parameterization.

6 Conclusions

We have examined the impact of CO_2-induced climate change on the evolution of mid-latitude baroclinic waves and associated water vapor transport and precipitation. Transient eddy behavior has been analyzed in a series of short-term numerical experiments that isolate the effects of climatic change of the zonal mean state from other feedbacks. Our integrations were initialized with the zonal-mean climate states for current and doubled CO_2 produced by the GFDL and NCAR general circulation models. Interpretation of extended GCM climate simulations can be assisted by this type of experimentation. In several instances the response in the GCM climate simulations can be explained on the basis on changes in the short-term evolution of transient eddies.

The smaller meridional temperature gradient in the doubled CO_2 climate leads to a reduction in eddy kinetic energy and sensible heat transport. Most of the reduction in eddy kinetic energy occurs in the the subtropics and is related to a substantial reduction in the equatorward propagation of eddy activity during the late stages of eddy development. Eddy kinetic energy and precipitation are shifted poleward as a consequence. Meridional transport of water vapor also shifts slightly poleward, but exhibits a comparatively small change in magnitude due to the compensating effect of higher specific humidity in the altered climatic state. The mean meridional circulation generated by the eddy also provides a negative feedback, so that the change in the total dynamical transport of water vapor is quite small. Precipitation in the lower mid-latitudes and subtropics decreases significantly, in both convection and large-scale supersaturation, even though relative humidity changes little so that specific humidity is higher in the doubled-CO_2 climate. The reduction in precipitation is related to the substantial reduction of eddy energy at those latitudes.

Because climate changes in the eddy transport of water vapor and eddy-generated precipitation are subtle, they are sensitive to model resolution. Our results suggest that a minimally acceptable truncation for a spectral model is rhomboidal 30. Adequate modeling of moisture flux from the surface is also essential in representing the modification of extratropical precipitation due to CO_2 doubling. Our results show that surface evaporation amplifies climatic changes in precipitation associated with mid-latitude waves.

Climate models which are less complex than GCMs may require some simple representation of the hydrological cycle. However, very little work has been done on parameterizing eddy moisture transports. Our results suggest that a successful parameterization must include the effects of nonlinear modification of the eddy and its environment and the frictional effects at the lower boundary. Parameterizations can be evaluated, in part, by comparison with life-cycle experiments.

Acknowledgments. The investigators thank W. Washington of NCAR and S. Manabe of GFDL for providing output from GCM climate experiments, R. Wetherald of GFDL and L. Ver Plank of NCAR for answering questions about the GCM output, D. Stewart of EDR for computing assistance, and P. Stone for useful comments on the manuscript. The research was supported by the NSF Climate Dynamics and Large Scale Dynamics Programs (grant ATM-8815290) and NASA's Global Scale Atmospheric Processes Research Program (grant NAG8-656).

References

Blackmon ML, White GH (1982) Zonal wavenumber characteristics of Northern Hemisphere transient eddies. J Atmos Sci 39: 1985-1998

Bourke W (1974) A multi-level spectral model. I. Formulation and hemispheric integrations. Mon Wea Rev 102:687-701

Branscome LE (1983) A parameterization of transient eddy heat flux on a beta-plane. J Atmos Sci 40:2508-2521

Branscome LE, Gutowski WJ, Stewart DA (1989) Effect of surface fluxes on the nonlinear development of baroclinic waves. J Atmos Sci 46:460-475

Brenner S, Yang CH, Yee SY (1982) The AFGL spectral model of the moist global atmosphere: Documentation of the baseline version. AFGL-TR-82-0393, NTIS ADA 129283, 65 pp

Edmon HJ, Hoskins BJ, McIntyre ME (1980) Eliassen-Palm cross-sections for the troposphere. J Atmos Sci 37:2600-2616

Gall RL (1976) Structural changes in growing baroclinic waves. J Atmos Sci 33:374-390

Grell GA, Kuo YH, Pasch RJ (1991) Semiprognostic tests of cumulus parameterization schemes in the middle latitudes. Mon Wea Rev 119:5-31

Gutowski WJ, Branscome LE, Stewart DA (1989) Mean flow adjustment during life cycles of baroclinic waves. J Atmos Sci 46:1724-1737

Gutowski WJ, Branscome LE, Stewart DA (1991a) Life cycles of moist baroclinic eddies. J Atmos Sci (submitted)

Gutowski WJ, Gutzler DS, Wang WC (1991b) Surface energy balances of three

general circulation models: Implications for simulating regional climate change. J Climate 4:121-134

Kuo H (1974) Further studies of the parameterization of the influence of cumulus convection on large-scale flow. J Atmos Sci 31:1232-1240

Hansen J, Lacis A, Rind D, Russell G, Stone P, Fung I, Ruedy R, Lerner J (1984) Climate sensitivity: Analysis of feedback mechanisms. In: Hansen J, Takahashi T (eds) Climate processes and climate sensitivity. AGU, Washington DC, 130-163

Krishnamurti TN, Kanamitsu M,Godbole R, Chang CB, Carr F, Chow JH (1976) Study of a monsoon depression (II), dynamical structure. J Meteor Soc Japan 54:208-225

Leovy CB (1973) Exchange of water vapor between the atmosphere and surface of Mars. Icarus 18:120-125

Manabe S, Wetherald R (1975) The effects of doubling the CO_2 concentration on the climate of a general circulation model. J Atmos Sci 32:3-15

Manabe S, Wetherald R (1980) On the distribution of climate change resulting from an increase in CO_2 content. J Atmos Sci 37:99-118

Manabe S, Wetherald R (1985) CO_2 and hydrology. Adv Geophysics 28:131-158

Manabe S, Wetherald R (1987) Large-scale changes of soil wetness induced by an increase in atmospheric carbon dioxide. J Atmos Sci 44:1211-1235

Michaud R, Derome J (1991) On the mean meridional transport of energy in the atmosphere and oceans as derived from six years of ECMWF analysis. Tellus 43A:1-14

Oort A (1983) Global atmospheric circulation statistics, 1958-1973. NOAA prof.

paper 14. Dept of Commerce, Washington DC,180 pp

Phillips NA (1979) The nested grid model. NOAA Technical Report NWS-22, Dept of Commerce, Washington DC, 79 pp

Pitcher EJ, Malone RC, Ramanathan V, Blackmon ML, Puri K, Bourke W (1983) January and July simulations with a spectral general circulation model. J Atmos Sci 40:580-604

Schlesinger ME, Mitchell JFB (1987) Climate model simulations of the equilibrium climatic response to increased carbon dioxide. Rev Geophys 25:760-798

Schneider EK (1981) On the amplitudes reached by baroclinically unstable disturbances. J Atmos Sci 38:2142-2149

Sela JG (1980) Spectral modeling at the National Meteorological Center. Mon Wea Rev 108:1279-1291

Simmons AJ, Hoskins BJ (1978) The life-cycles of some nonlinear baroclinic waves. J Atmos Sci 35:414-432

Stone PH, Yao MS (1990) Development of a two-dimensional zonally averaged statistical-dynamical model. Part III: The parameterization of the eddy fluxes of heat and moisture. J Climate 3:726-740

Stone PH, Yao MS (1991) Vertical eddy heat fluxes from model simulations. J Climate 4:304-317

Ulbrich U, Speth P (1991) The global energy cycle of stationary and transient atmospheric waves: Results from ECMWF analyses. Meteorol Atmos Phys 45:125-138

Washington W, Meehl G (1984) Seasonal cycle experiment on the climate

sensitivity due to the doubling of CO_2 with an atmospheric general circulation model coupled to a simple mixed-layer ocean model. J Geophys Res 89:9475-9503

Figure Legends

Fig. 1. Zonal mean 950 hPa temperatures (top) from GFDL GCM and NCAR CCM climate simulations for Northern Hemisphere winter with present-day amount of CO_2 ($1xCO_2$). The bottom figure shows the difference between the temperatures in the climate simulations with doubled ($2xCO_2$) and present-day CO_2.

Fig. 2. As in Fig. 1, but for vertical and zonal mean specific humidity.

Fig. 3. Time series of eddy kinetic energy, expressed as hemispheric mean velocity variance, from experiments using the GFDL GCM (top) and NCAR CCM (bottom) zonal mean climates as initial conditions.

Fig. 4. Latitudinal distribution of eddy kinetic energy, expressed as hemispheric mean velocity variance, from experiments using the NCAR CCM climates as initial conditions. Data is taken from day 20 of the integrations (shown at bottom of Fig. 3), which is the day of maximum eddy kinetic energy.

Fig. 5. Vertical and zonal mean eddy flux of specific humidity from experiments using the GFDL (top) and NCAR (bottom) climates as initial conditions. Flux is averaged in time over eddy life cycle. Observed transient eddy flux for Northern Hemisphere winter (Oort 1983) is also shown (top).

Fig. 6. Vertical and zonal mean total specific humidity flux by the eddy and mean meridional circulation in experiments using the GFDL (top) and NCAR (bottom) climates as initial conditions. Flux is averaged in time over eddy life cycle.

Fig. 7. Zonal mean precipitation due to large-scale condensation, occurring over

eddy life cycles in experiments using GFDL (top) and NCAR (bottom) climates as initial conditions.

Fig. 8. Zonal mean precipitation due to moist convection, occurring over eddy life cycles in experiments using NCAR climates as initial conditions.

Fig. 9. Vertical and zonal mean eddy flux of specific humidity (top) and large-scale precipitation (bottom) using GFDL climates as initial conditions in experiments with meridional resolution equivalent to rhomboidal 15 truncation. Flux is averaged over eddy life cycle, precipitation is total amount over life cycle.

Fig. 10. Vertical and zonal mean eddy flux of specific humidity (top) and large-scale precipitation (bottom) using GFDL climates as initial conditions in experiments with standard meridional resolution and no surface evaporation. ΔT Only experiment uses temperature from $2xCO_2$ climate and specific humidity from $1xCO_2$ climate as initial state. Flux is averaged over eddy life cycle, precipitation is total amount over life cycle.

Fig. 11. Vertical, zonal and time mean eddy flux of specific humidity from experiments using GFDL climates as initial conditions, compared with flux calculated from parameterization of Stone and Yao (1990) using GFDL climates as input.

Fig. 12. Vertical profile of zonal and time mean eddy flux of specific humidity at 30°N from experiment using $1xCO_2$ GFDL climate as initial condition, parameterization using $1xCO_2$ and $2xCO_2$ GFDL climates as input, and observations of Oort (1983).

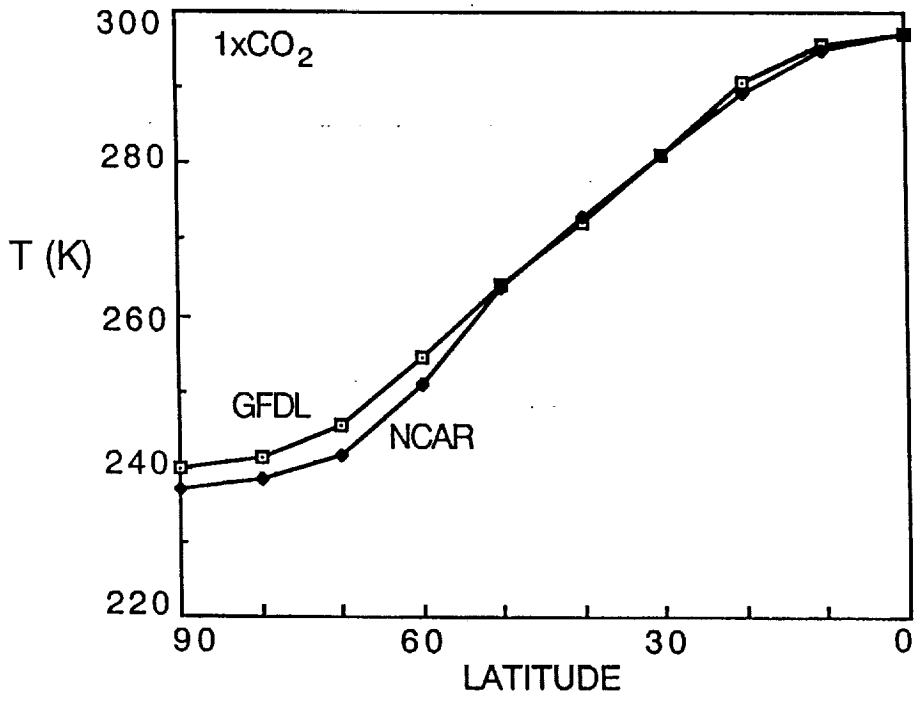
300
280
260
240
220
T (K)
1xCO2
GFDL
NCAR
90
60
30
0
LATITUDE

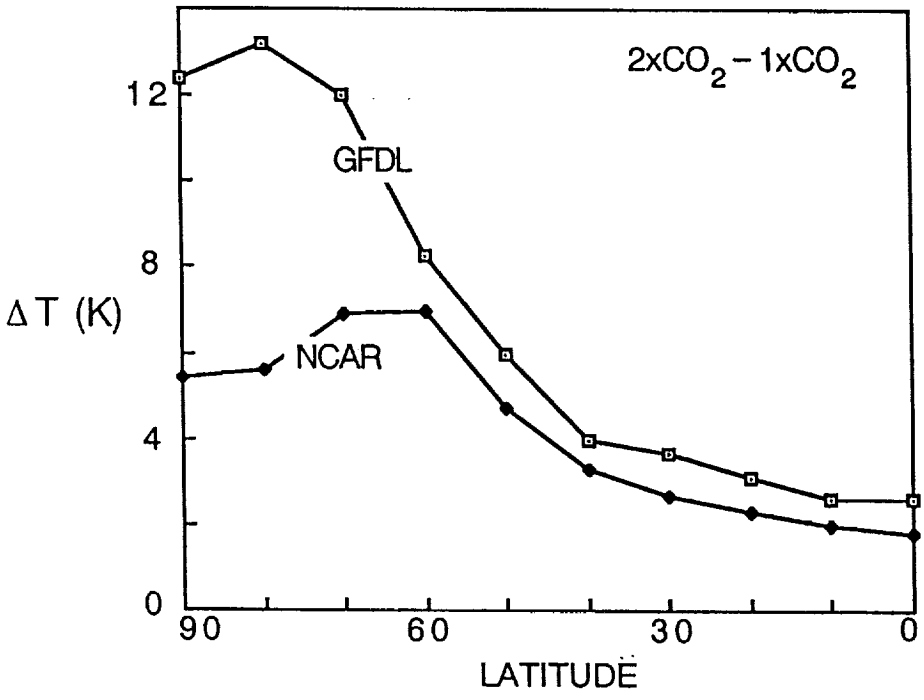
12
8
4
0
ΔT (K)
2xCO2 – 1xCO2
GFDL
NCAR
90
60
30
0
LATITUDE

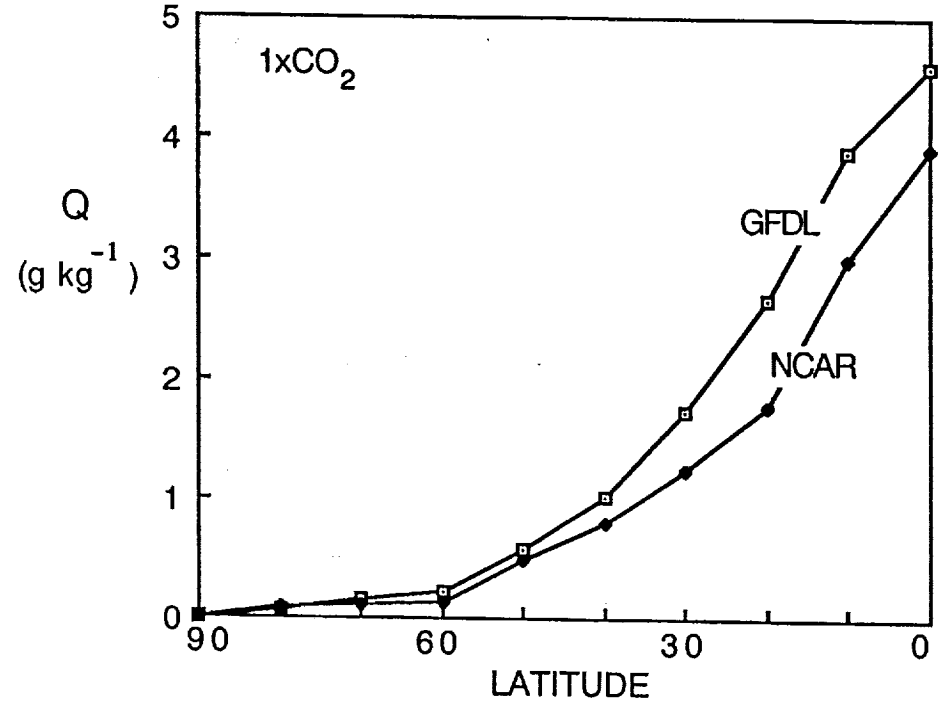
1xCO2
Q
(g kg-1)
GFDL
NCAR
5
4
3
2
1
0
90
60
30
0
LATITUDE

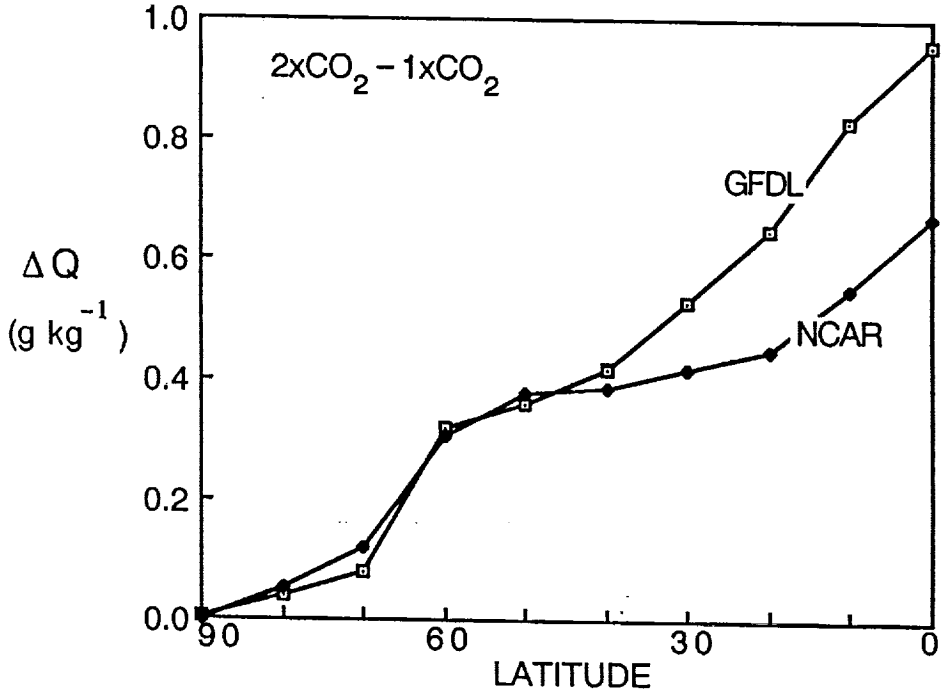
2xCO2 – 1xCO2
ΔQ
(g kg-1)
GFDL
NCAR
1.0
0.8
0.6
0.4
0.2
0.0
90
60
30
0
LATITUDE

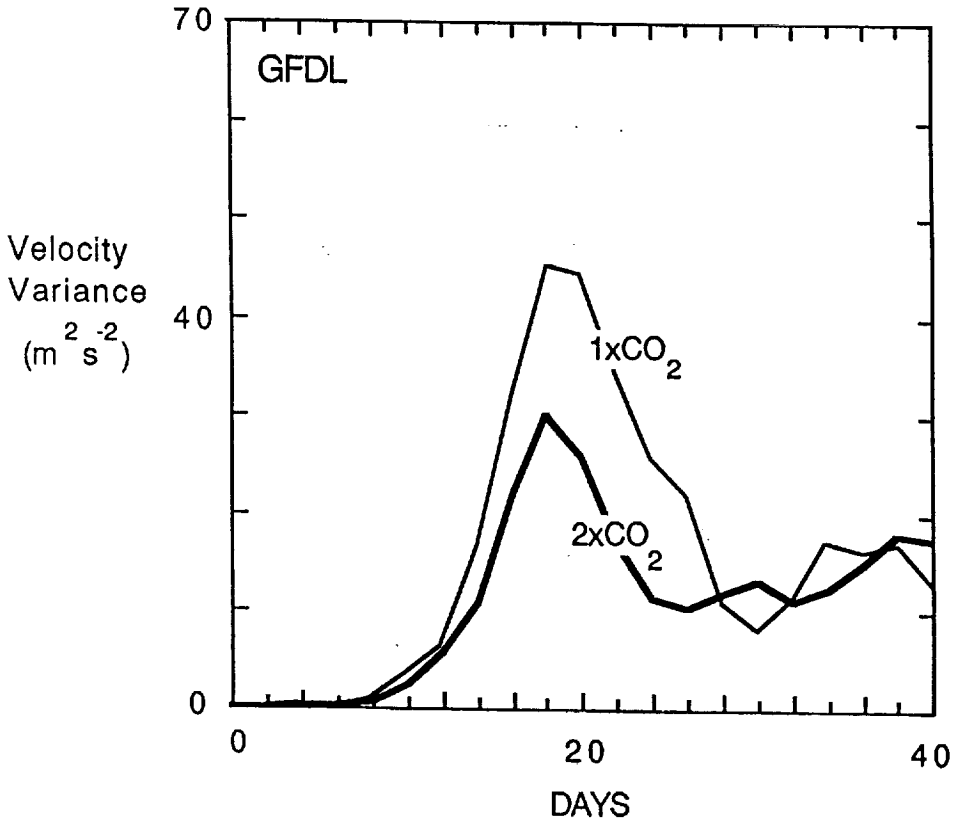
GFDL
Velocity Variance ($m^2 s^{-2}$)
70
40
0
1xCO2
2xCO2
0
20
40
DAYS

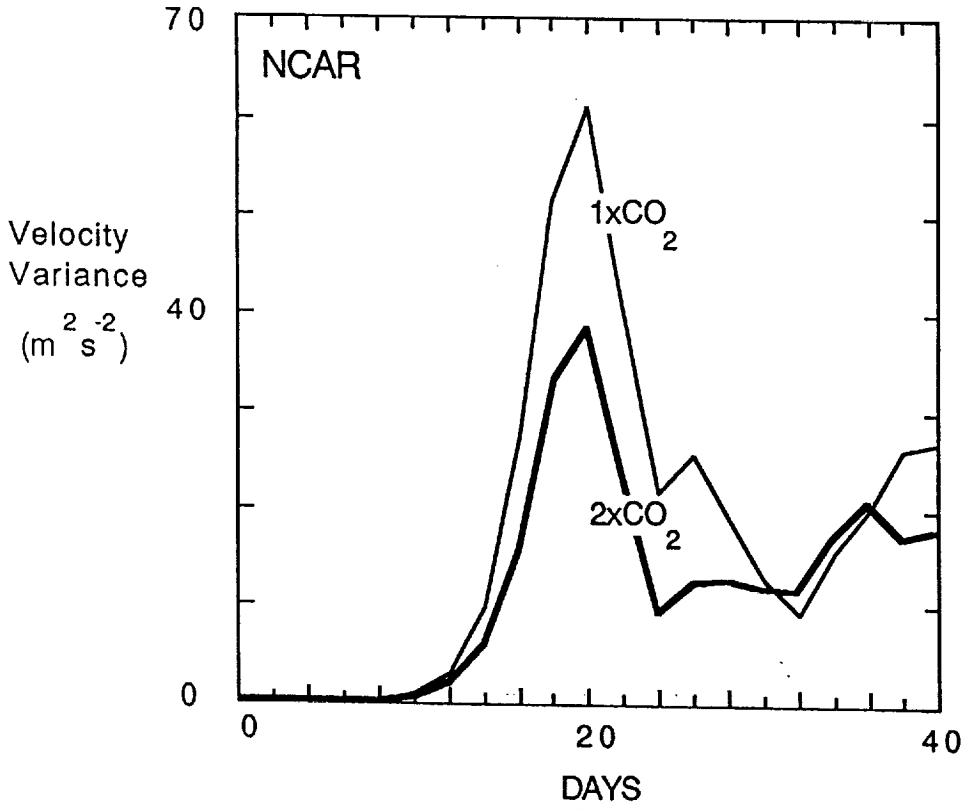
NCAR
Velocity Variance ($m^2 s^{-2}$)
70
40
0
1xCO2
2xCO2
0
20
40
DAYS

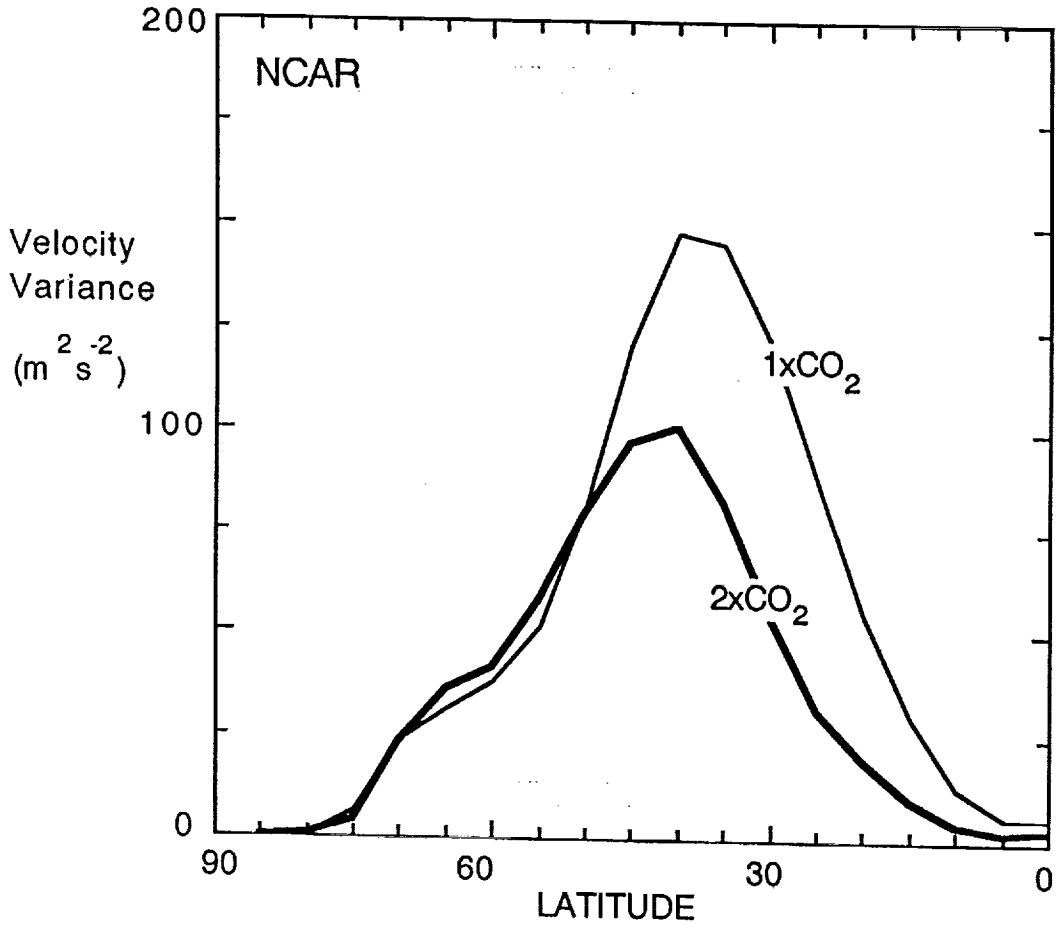
200
NCAR
Velocity
Variance
(m 2 s -2)
100
0
1xCO2
2xCO2
90
60
30
0
LATITUDE

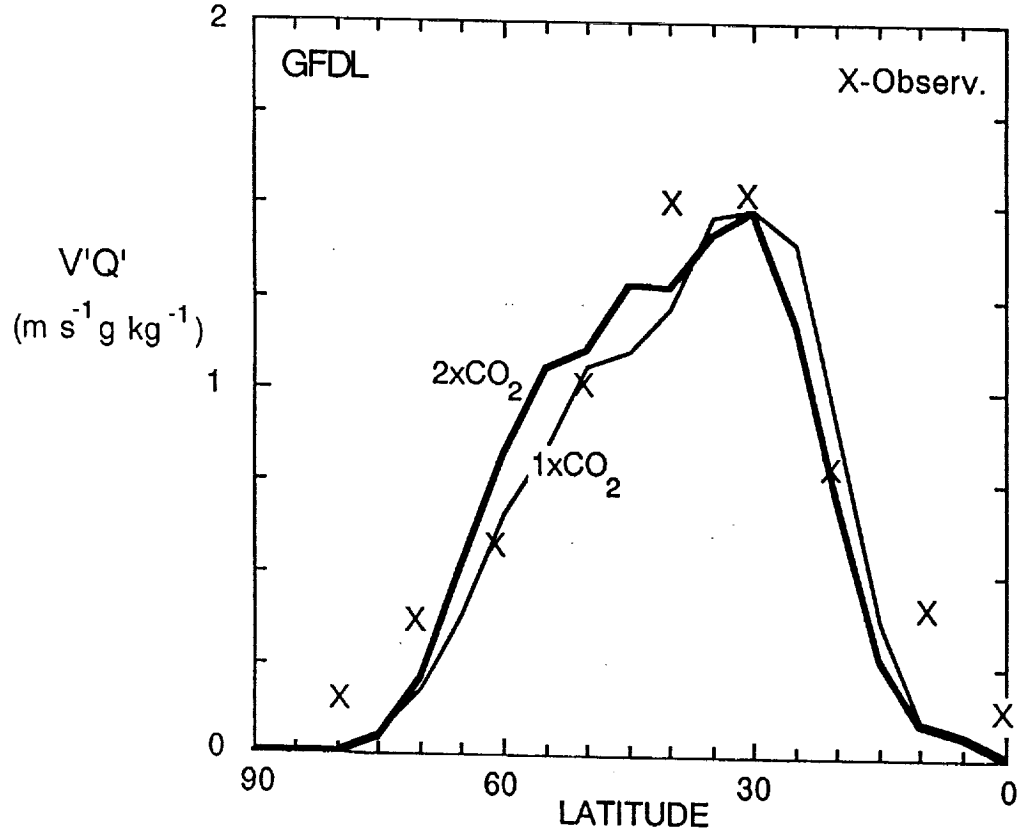
GFDL
X-Observ.
V'Q'
(m s-1 g kg-1)
2xCO2
1xCO2
2
1
0
90
60
30
0
LATITUDE

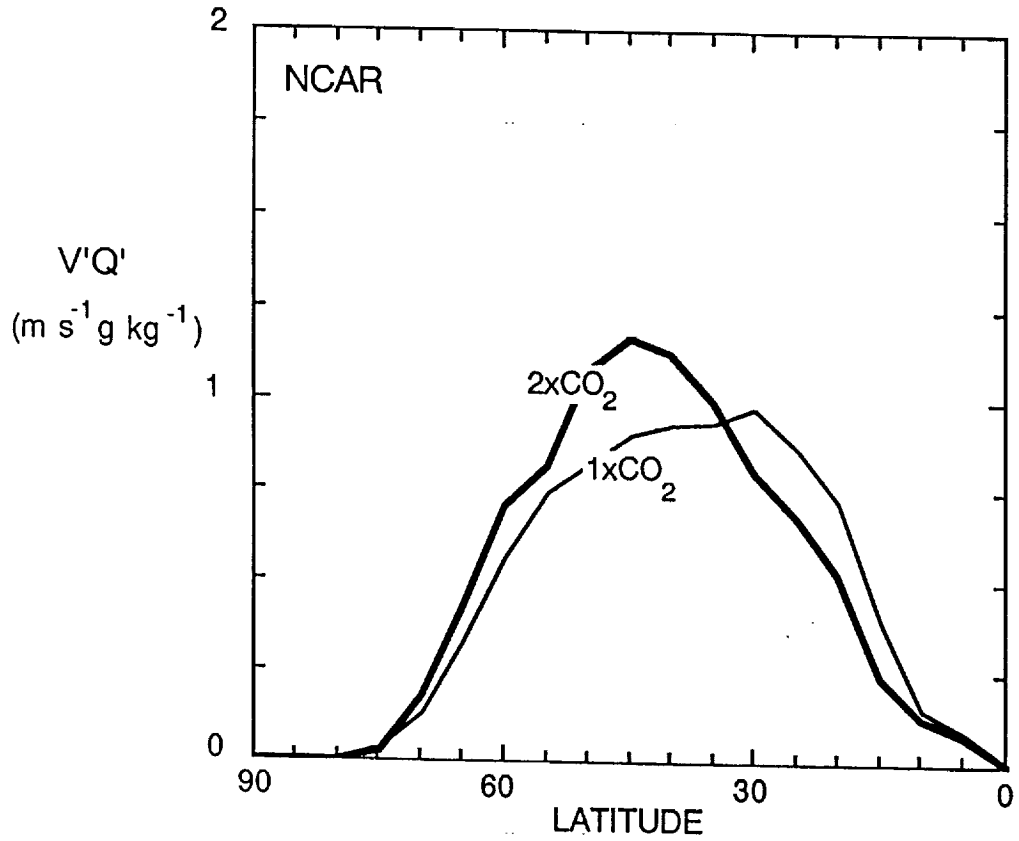
NCAR
V'Q'
(m s-1 g kg-1)
2xCO2
1xCO2
2
1
0
90
60
30
0
LATITUDE

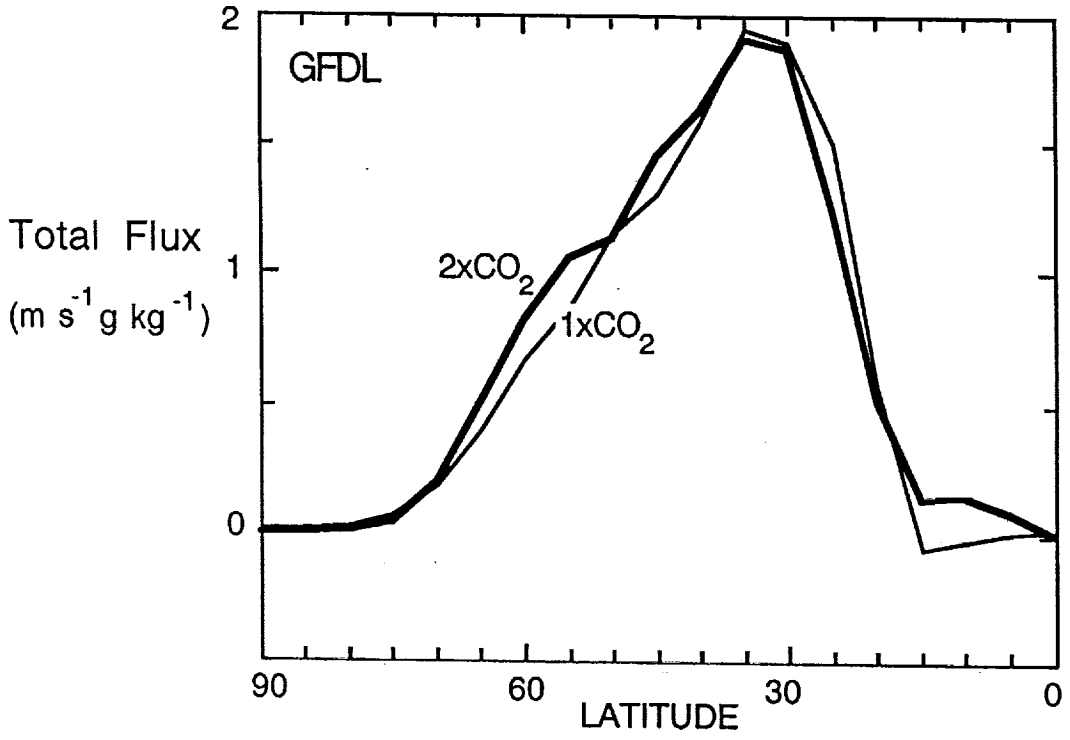
GFDL
Total Flux
(m s-1 g kg-1)
2xCO2
1xCO2
2
1
0
90
60
30
0
LATITUDE

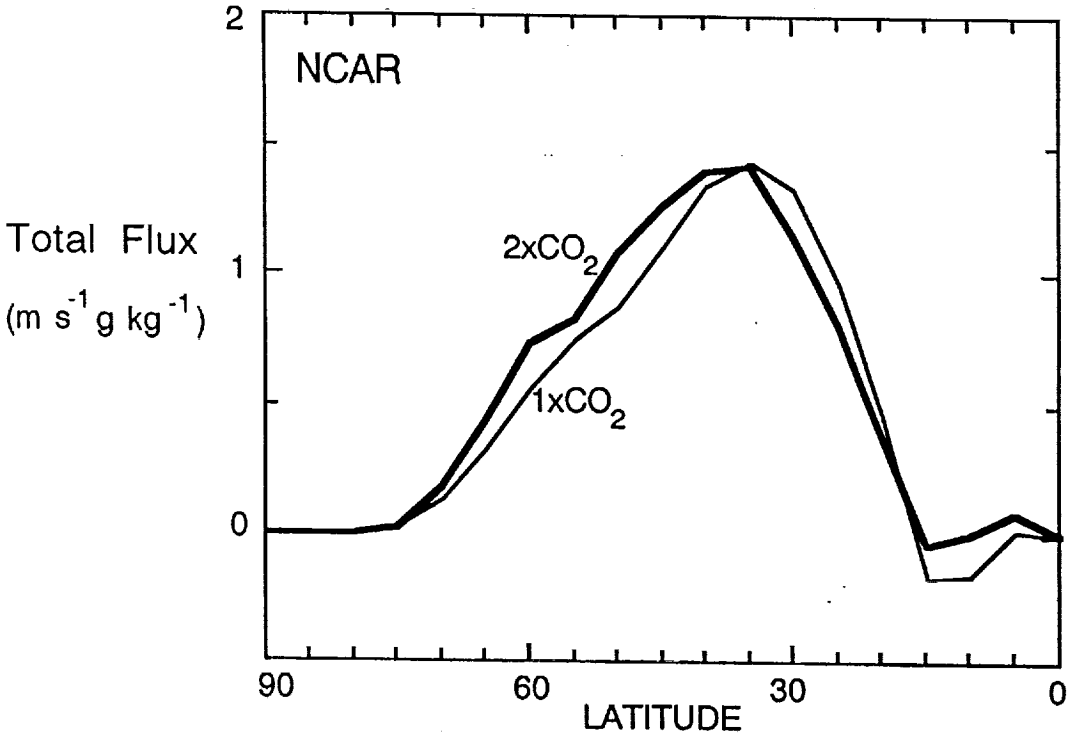
NCAR
Total Flux
(m s-1 g kg-1)
2xCO2
1xCO2
2
1
0
90
60
30
0
LATITUDE

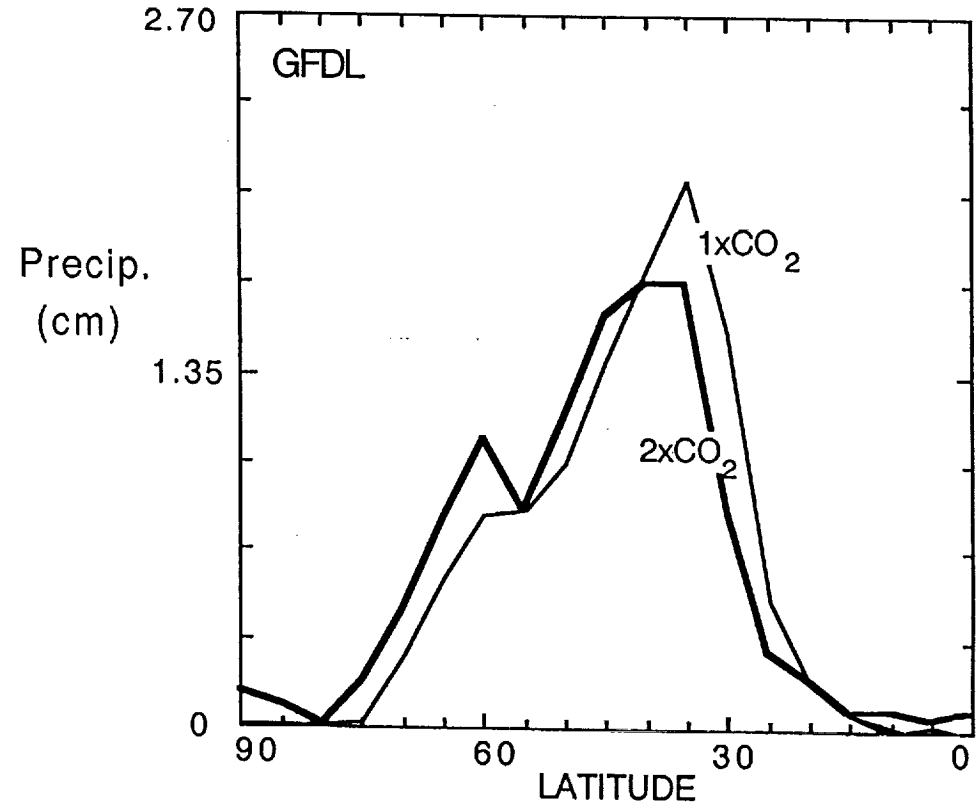
2.70
GFDL
Precip.
(cm)
1.35
0
1xCO2
2xCO2
90
60
30
0
LATITUDE

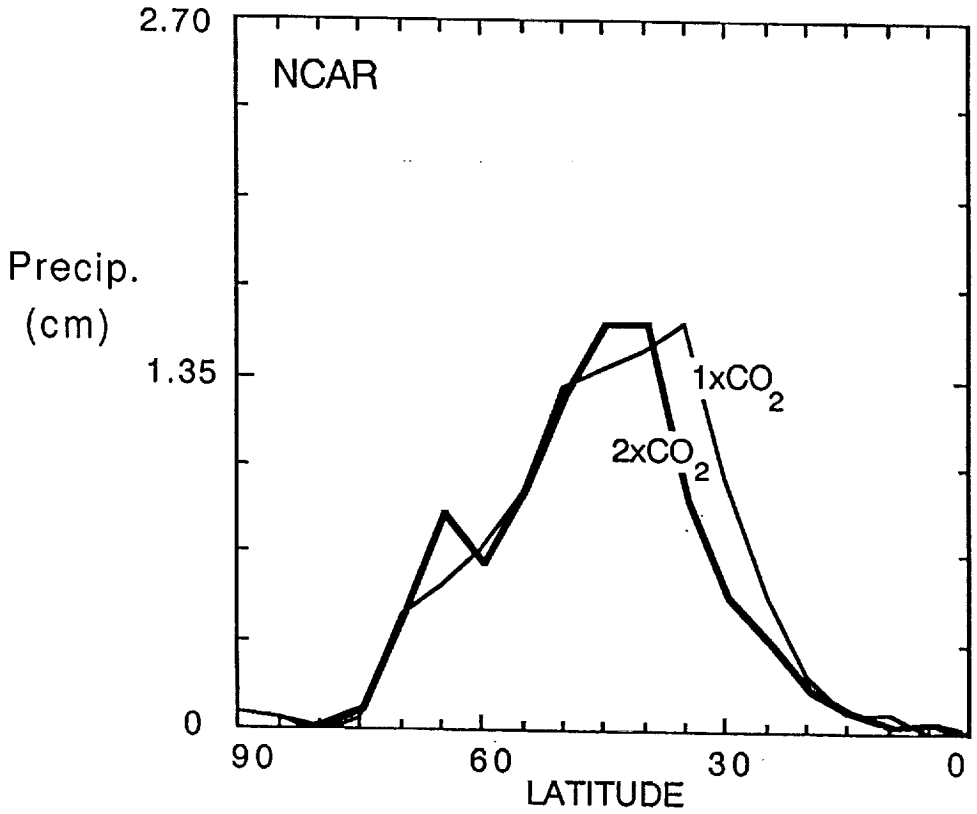
2.70
NCAR
Precip.
(cm)
1.35
0
1xCO2
2xCO2
90
60
30
0
LATITUDE

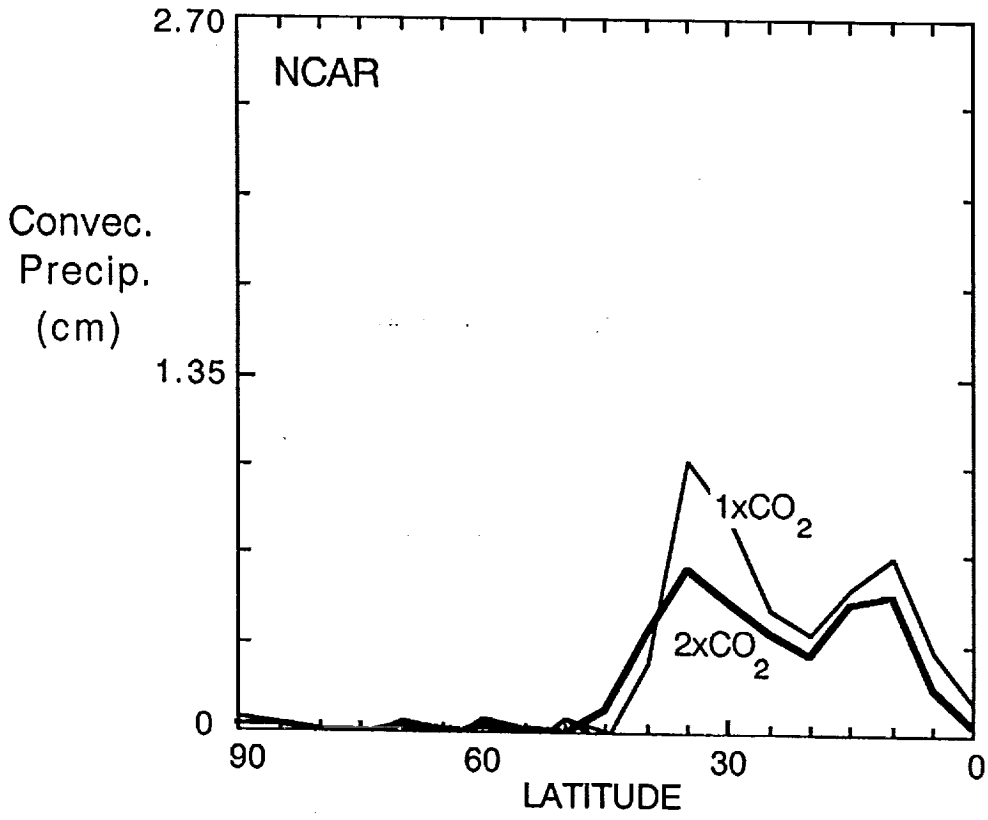
2.70
NCAR
Convec.
Precip.
(cm)
1.35
1xCO2
2xCO2
0
90
60
30
0
LATITUDE

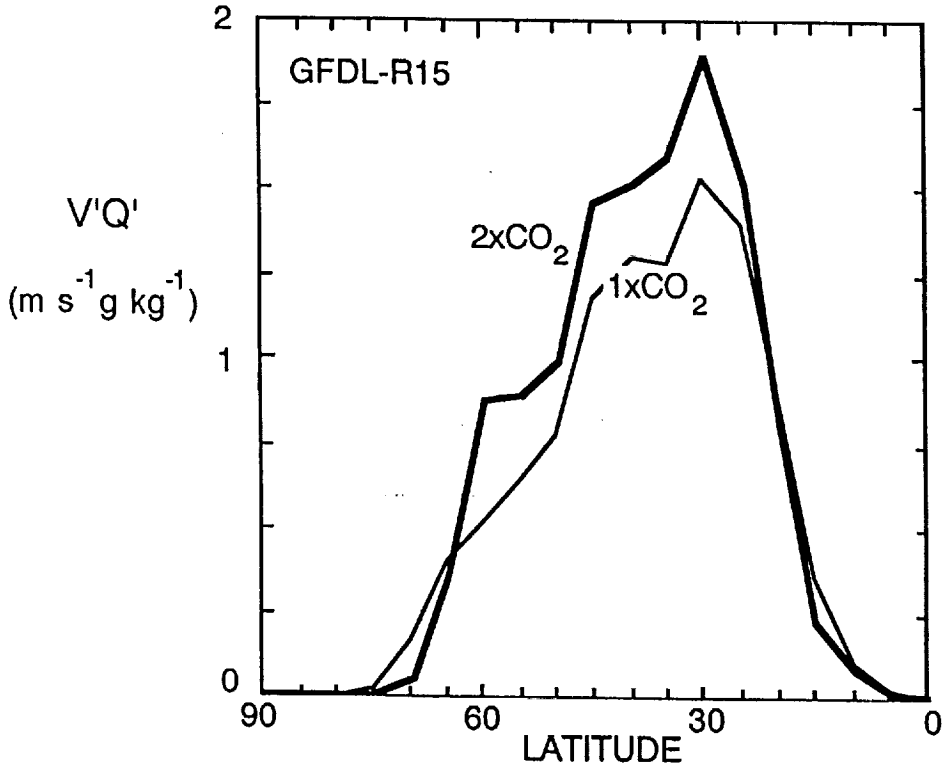
GFDL-R15
V'Q'
(m s^{-1} g kg^{-1})
2xCO$_2$
1xCO$_2$
2
1
0
90
60
30
0
LATITUDE

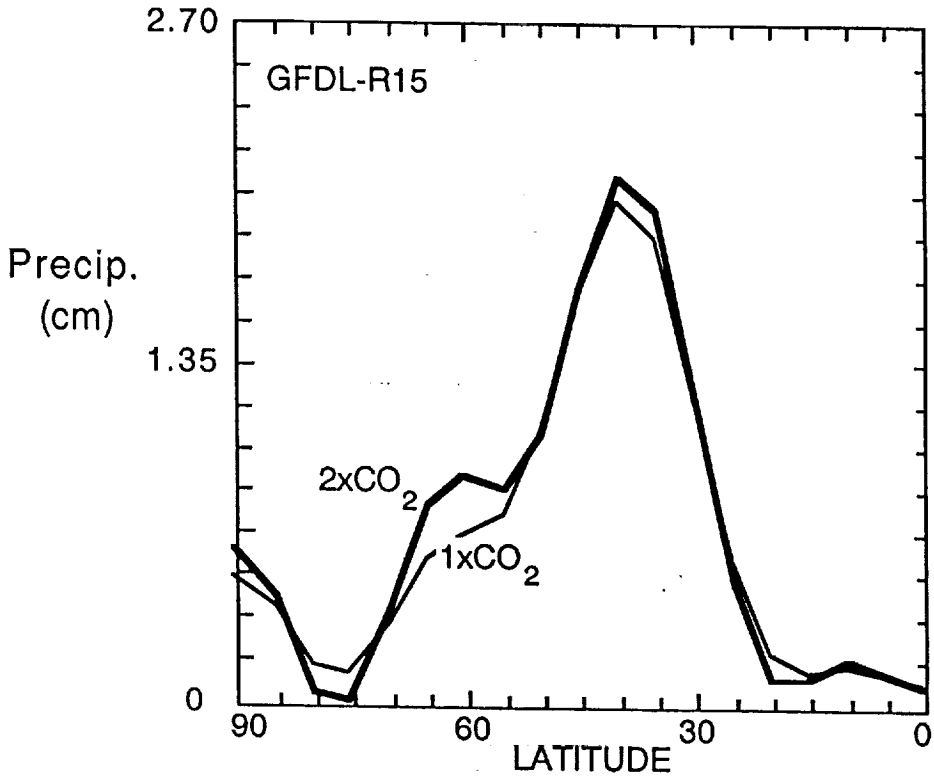
GFDL-R15
Precip.
(cm)
2.70
1.35
0
2xCO$_2$
1xCO$_2$
90
60
30
0
LATITUDE

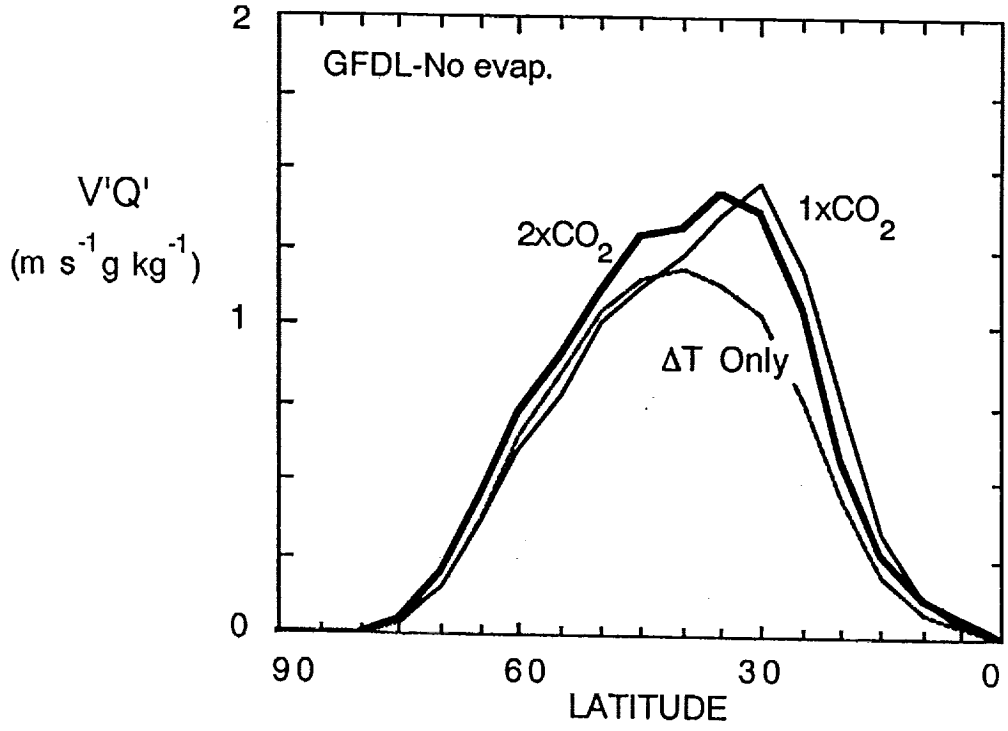
GFDL-No evap.
V'Q'
(m s-1 g kg-1)
2
1
0
2xCO2
1xCO2
ΔT Only
90
60
30
0
LATITUDE

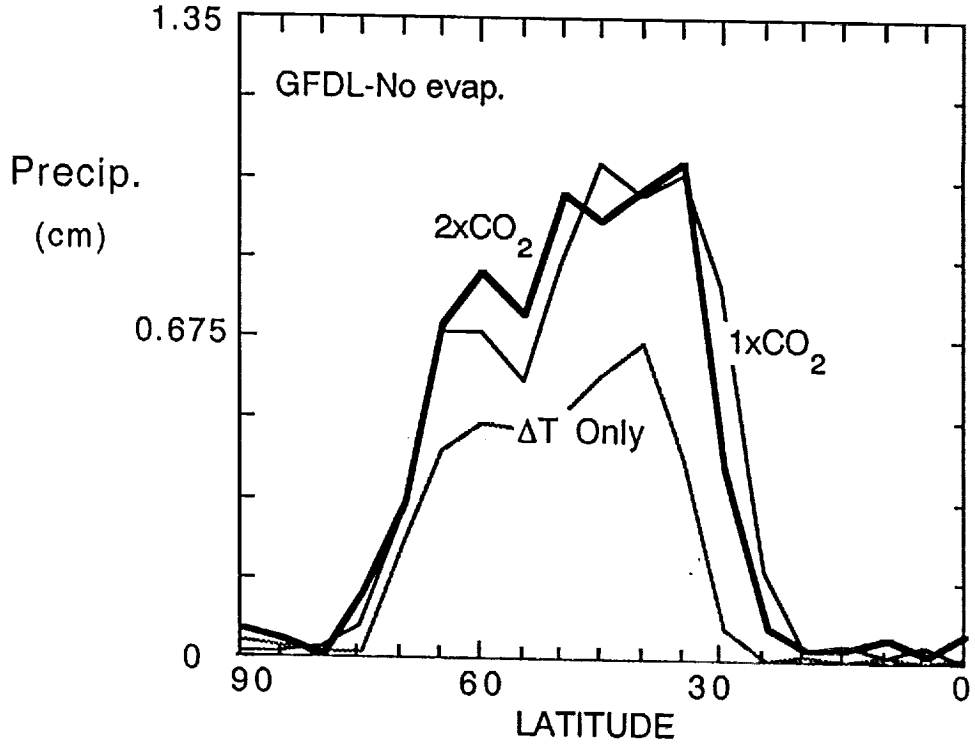
GFDL-No evap.
Precip.
(cm)
1.35
0.675
0
2xCO2
1xCO2
ΔT Only
90
60
30
0
LATITUDE

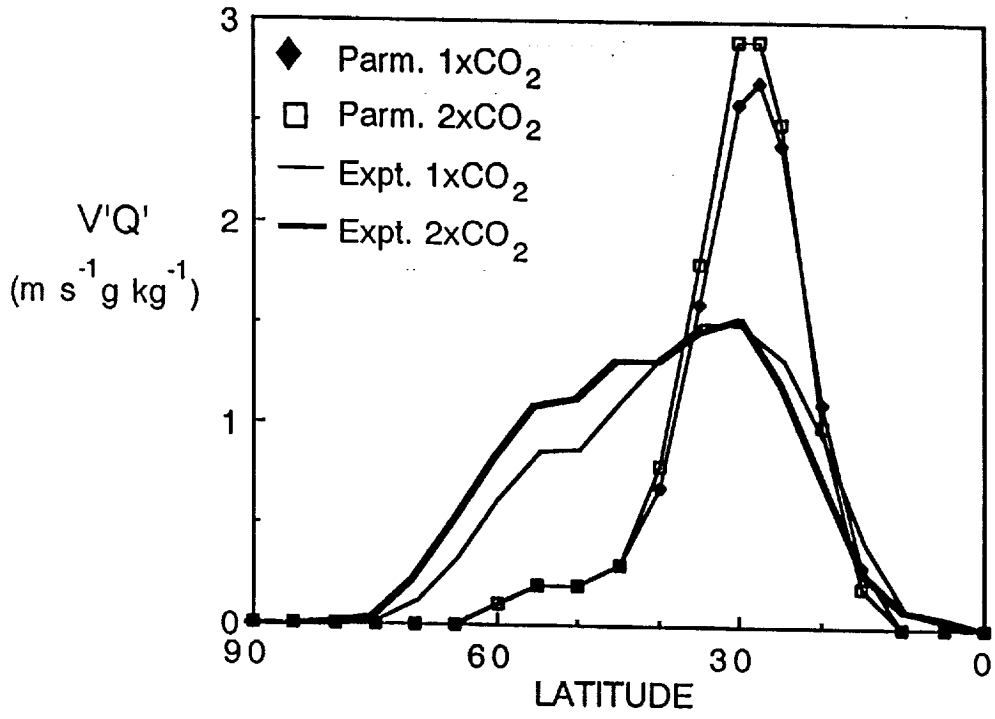
Parm. 1xCO2
Parm. 2xCO2
Expt. 1xCO2
Expt. 2xCO2
V'Q'
(m s-1 g kg-1)
3
2
1
0
90
60
30
0
LATITUDE

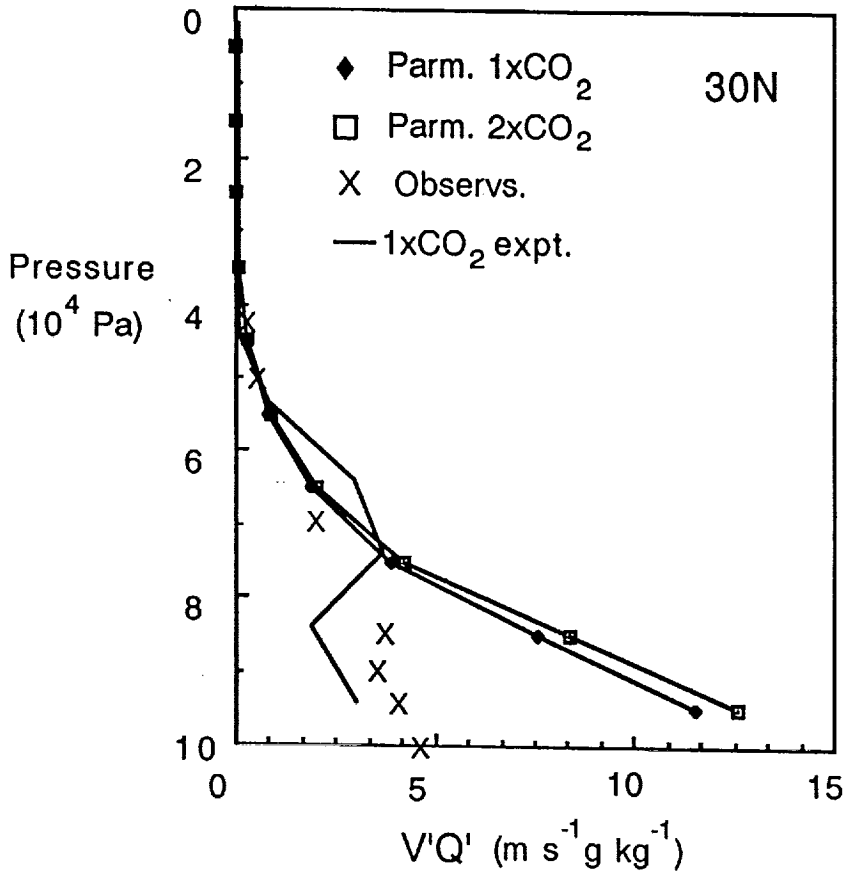
Parm. 1xCO2
Parm. 2xCO2
X Observs.
1xCO2 expt.
30N
Pressure
(10^4 Pa)
0
2
4
6
8
10
0
5
10
15
V'Q' (m s^-1 g kg^-1)